JOURNAL OF THERMOPHYSICS AND HEAT TRANSFER
Vol. 13, No. 1, January–March 1999

Generalized Finite Element–Harmonic Analysis for Nonlinear Heat Transfer

Dan Givoli* and Omri Rand*
Technion—Israel Institute of Technology, Technion City, 32000 Haifa, Israel

A numerical method is devised for the solution of nonlinear problems in bodies whose boundaries can be uniquely described in cylindrical coordinates. It provides a generalization of standard finite element (FE) Fourier analysis to nonlinear problems with asymmetric geometry and material properties. One class of problems in this category is that involving nonlinear steady-state heat transfer in a body with asymmetric geometry, thermal loading, and thermal properties. The proposed method combines FE discretization in a plane or interval and a symbolically implemented Fourier decomposition in the circumferential direction. Applications include space structures or structural members in space structures exposed to incoming solar heat flux and emitting thermal radiation.

Nomenclature

C_R	=	heat radiation coefficient
D	=	three-dimensional domain
$\boldsymbol{d}$	=	global finite element solution (temperature) vector, $\{d_I\}$
$\boldsymbol{d}^e$	=	solution (temperature) vector of element e, $\{d_i^e\}$
f	=	incident heat flux
g	=	prescribed surface temperature
M	=	number of degrees of freedom in the finite element analysis
N	=	number of harmonics in the Fourier expansion
N_{np}, N_{el}	=	number of nodal points, number of elements
$\boldsymbol{n}$	=	outward unit normal vector on boundary Γ
$\boldsymbol{n}_\gamma$	=	outward normal vector on boundary γ in the asymmetric case
r	=	radial coordinate
$T_1(\theta)$, $T_2(\theta)$	=	geometrical factors appearing in the asymmetric case, Eq. (19)
u	=	absolute temperature
w	=	weighting function
$\boldsymbol{x}$	=	location vector, (r, θ, z)
z	=	axial coordinate
Γ	=	boundary of D
Γ_H, Γ_T	=	parts of Γ where normal heat flux and temperature are prescribed
γ	=	boundary of Ω
γ_H, γ_T	=	parts of γ where normal heat flux and temperature are prescribed
θ	=	angular coordinate
κ	=	thermal conductivity tensor
$\bar{\kappa}$	=	thermal conductivity tensor in the (r, z) plane
κ_θ	=	thermal conductivity in the angular direction
λ	=	surface thermal convection coefficient
ϕ_i	=	finite element shape function
Ω	=	two-dimensional domain in the (r, z) plane
Ω^e	=	domain of element e
$\bar{\nabla}$	=	Cartesian gradient operator in the (r, z) plane

Received Nov. 14, 1997; revision received July 21, 1998; accepted for publication July 24, 1998. Copyright © 1998 by the American Institute of Aeronautics and Astronautics, Inc. All rights reserved.

*Associate Professor, Faculty of Aerospace Engineering.

I. Introduction

THE combined use of finite element (FE) discretization and Fourier analysis is quite common in various areas of aerospace engineering. A frequent case is that where Fourier decomposition is applied in time, and FEs are employed in space. Fourier decomposition in time is commonly used in structural, acoustics, and control analyses of aerospace structures. Applications include, e.g., the dynamic analysis of cylindrical structures,[1] the structural dynamics of rotating rotor blades,[2] the solution of fluid–structure interaction problems,[3] and the analysis of rotating space structures.[4–6]

Another method in the same category is the spectral element Fourier method that combines Fourier expansions with spectral elements or with p-type FEs. See the application of the method to the Navier–Stokes equations in Ref. 7 and to the time-dependent heat equation in Ref. 8. A related class of methods has been discussed in Ref. 9. Also see Ref. 10 for a review of p-type methods.

Another important case where a Fourier-based (spectral) method and the FE method are combined, is the time-independent analysis of axisymmetric bodies, i.e., bodies of revolution, under asymmetric loads. In this case, Fourier decomposition is applied in the angular (circumferential) direction, whereas FEs are used in the axial and radial directions. In this paper, this combined method will be called the Fourier finite element (FFE) method. Some computational issues regarding FFE are discussed in Refs. 11 and 12. The use of FFE in the analysis of linear elastic axisymmetric structures loaded by asymmetric loads is reported in Refs. 13–15.

The FFE method has several advantages, the main one being the dimensional reduction in the FE formulation, which leads to a reduction in the complexity of the numerical model. This includes the meshing process, which has to be done in a lower dimension, e.g., a two-dimensional mesh instead of a three-dimensional mesh. Also, in many cases, in particular when the solution is sufficiently smooth in the angular direction, i.e., the loading can be described by a small number of harmonics, FFE is computationally more efficient, namely it can achieve the same accuracy as a full FE model, with a smaller number of degrees of freedom. Up to now, the application of this method has been restricted to the case of asymmetric loads with axisymmetric geometry.

Most of the work employing FFE is related to linear problems,[11–15] whereby the different modes are decoupled and superposition of solutions generated by the different Fourier components of the loading is possible. However, a few papers discuss the extension of FFE to the nonlinear regime. Refer-

ences 16–19 propose FFE schemes for large deformation problems of axisymmetric solids and shells under general loading. In Ref. 20, the authors develop an FFE procedure for nonlinear steady-state thermal analysis of large truss-type space structures with thin-walled members.

In this paper, a new FFE method for nonlinear problems is proposed, which, in several respects, is an extension of the schemes in Refs. 16–19. The present method is based on a nonstandard variational (virtual-work) form of the problem and FE formulation, in cylindrical coordinates, which lead to a system of semidiscrete equations with respect to the angular direction. This system has a remarkable resemblance to a dynamic semidiscrete system in transient analysis. This set of differential equations is solved using a harmonic balance procedure, which is implemented using a special-purpose symbolic manipulation library of subroutines.[4,20] In addition, the present FFE method easily handles asymmetric geometries, namely domains that deviate from bodies of revolution. The only theoretical restriction required of the geometry is that the inner and outer boundaries of the given body be represented continuously and be uniquely defined in cylindrical coordinates. The material properties are also allowed to be asymmetric.

The proposed method is developed in this paper in the context of nonlinear steady-state thermal analysis of a solid body. This is chosen as a model to bring to light the special features of the new method, although the method can be applied in principle to other types of problems as well, e.g., to nonlinear structural problems. The nonlinearity of the problem is caused by the presence of thermal radiation and possibly also temperature-dependent thermal conductivities. One relevant application is the thermal analysis of thick shell structures, or the analysis of specific members in space structures, exposed to incoming solar heat flux and emitting thermal radiation, when a detailed local analysis is required. The results of such analysis can serve as input to a thermoelastic analysis, which can also be performed using the same FFE methodology.

Following is the outline of the paper. In Sec. II, the FE formulation is derived for the case of a body of revolution. The nonlinear symbolic analysis in the angular direction is also briefly addressed. In Sec. III, it is shown how this formulation can easily be extended to more general geometries. In Sec. IV, the two-dimensional case is considered, and explicit expressions are obtained for the element matrices and vectors with linear FE shape functions. The numerical examples given in Sec. V demonstrate the performance of the method. Some computational aspects of the method are also discussed. The paper is concluded with several remarks in Sec. VI.

II. FE Formulation for Bodies of Revolution

Consider the problem of finding the steady-state temperature distribution u in a three-dimensional solid body, made of an anisotropic material, and occupying the domain D. The boundary of D is denoted Γ. Initially, it will be assumed that D is a body of revolution, i.e., has axisymmetric geometry, but in the next section this assumption will be relaxed (Fig. 1a). The cylindrical coordinate system (r, θ, z) is used, where z is the axis of symmetry. In D, the nonlinear steady-state heat equation governs, namely

$$\nabla \cdot \kappa(\boldsymbol{x}, u)\nabla u = 0 \quad \text{in} \quad D \tag{1}$$

The thermal conductivity tensor κ may be a function of location $\boldsymbol{x} = (r, \theta, z)$ and of temperature, as indicated in Eq. (1). It has the general symmetric form

$$\kappa = \begin{bmatrix} \kappa_r & 0 & \kappa_{rz} \\ 0 & \kappa_\theta & 0 \\ \kappa_{rz} & 0 & \kappa_z \end{bmatrix} \tag{2}$$

It is assumed that the dependence of κ on u and θ (if it exists) is continuous, although κ may depend on r and z discontinuously, e.g., different materials in different regions in the (r, z) plane. Note also that in the (r, θ) plane, the polar coordinates are assumed to be the principal conductivity directions. Thus, we exclude material fibers that are oblique to the (r, θ) coordinates. These assumptions are needed so that the treatment of the θ direction can be separated later from that of the (r, z) plane.

The boundary Γ is divided into two parts: $\Gamma = \Gamma_H \cup \Gamma_T$. This subdivision must be uniform in the angle θ. On Γ_H, the normal heat flux is given, whereas on Γ_T, the temperature is prescribed. Thus, the boundary conditions are

$$\boldsymbol{n} \cdot \kappa \nabla u = f - \lambda u - C_R u^4 \quad \text{on} \quad \Gamma_H \tag{3}$$

$$u = g \quad \text{on} \quad \Gamma_T \tag{4}$$

The three terms on the right side of Eq. (3) represent the incident heat flux, surface thermal convection, and heat radiation. The data f, λ, C_R, and g may be functions of location (r, θ, z).

The problem [Eqs. (1–4)] is now rewritten in a weak form, to be approximated by the FE method. However, in contrast to the standard three-dimensional case, the FE formulation is applied here with respect to r and z only, whereas θ remains a continuous variable. To this end, D and its boundary Γ are decomposed via

$$\begin{aligned} D &= \Omega \times (0, 2\pi), \qquad \Gamma = \gamma \times [0, 2\pi] \\ \Gamma_H &= \gamma_H \times (0, 2\pi), \qquad \Gamma_T = \gamma_T \times (0, 2\pi) \end{aligned} \tag{5}$$

(Fig. 1b). The Cartesian gradient operator in the (r, z) plane is defined as follows:

$$\bar{\nabla} = \boldsymbol{e}_r \frac{\partial}{\partial r} + \boldsymbol{e}_z \frac{\partial}{\partial z} \tag{6}$$

where $\boldsymbol{e}_r$ and $\boldsymbol{e}_z$ are fixed unit vectors in the r and z directions, respectively. In addition, the conductivity tensor $\bar{\kappa}$ is defined

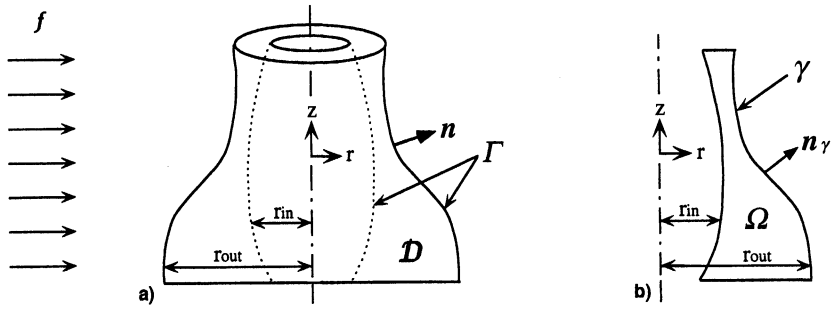

Fig. 1 Body of revolution: a) the three-dimensional domain and b) the two-dimensional domain in the (r, z) plane.

as the 2 × 2 part of κ in Eq. (2) in the (r, z) plane. Finally, the trial space $\mathcal{S}$ and the test space $\mathcal{S}_0$ are defined by

$$\mathcal{S} = \{u(r, \theta, z) | u \quad \text{continuous and} \quad u = g \quad \text{on} \quad \gamma_T\} \tag{7}$$

$$\mathcal{S}_0 = \{w(r, z) | w \quad \text{continuous and} \quad w = 0 \quad \text{on} \quad \gamma_T\} \tag{8}$$

Then the weak form of Eqs. (1–4) is as follows.

Find $u \in \mathcal{S}$ such that for all $w \in \mathcal{S}_0$

$$\int_\Omega \bar{\nabla} w \cdot \bar{\kappa} \bar{\nabla} u r \, d\Omega - \int_\Omega \frac{1}{r} w \frac{\partial}{\partial \theta} \left(\kappa_\theta \frac{\partial u}{\partial \theta} \right) d\Omega + \int_{\gamma_H} w(\lambda u + C_R u^4) r \, d\gamma = \int_{\gamma_H} w f r \, d\gamma \tag{9}$$

This equation is obtained by multiplying Eq. (1) by the weight wr, integrating over Ω, integrating by parts, and using Eq. (3).

Next, an FE mesh is introduced in the domain Ω, with N_{np} nodal points and N_{el} elements. The total number of degrees of freedom (excluding those associated with the prescribed temperatures on γ_T) is denoted M. The function u is replaced by the FE approximation

$$u^h(r, \theta, z) = \sum_{I=1}^{N_{np}} d_I(\theta) \phi_I(r, z) \tag{10}$$

where I indicates a node number, and ϕ_I is the global shape function associated with node I. The coefficients d_I are the nodal solutions, which are functions of θ. Following the Galerkin procedure, u^h given by Eq. (10) is substituted into Eq. (9), and w is replaced by the shape functions ϕ_J, for $J = 1, \ldots, M$. This leads to a system of ordinary differential equations in $\boldsymbol{d}(\theta)$. Using a superposed dot to indicate differentiation with respect to θ, this system has the form

$$M\ddot{\boldsymbol{d}}(\theta) + C\dot{\boldsymbol{d}}(\theta) + K\boldsymbol{d}(\theta) + \boldsymbol{Q}[\boldsymbol{d}(\theta)] = \boldsymbol{F}(\theta) \tag{11}$$

The global matrices M, C, and K, and the global vectors $\boldsymbol{Q}$ and $\boldsymbol{F}$ are calculated by assembling element contributions

$$M = \mathcal{A}_{e=1}^{N_{el}} m^e, \qquad C = \mathcal{A}_{e=1}^{N_{el}} c^e, \qquad K = \mathcal{A}_{e=1}^{N_{el}} k^e$$
$$\boldsymbol{Q} = \mathcal{A}_{e=1}^{N_{el}} \boldsymbol{q}^e, \qquad \boldsymbol{F} = \mathcal{A}_{e=1}^{N_{el}} \boldsymbol{f}^e \tag{12}$$

where $\mathcal{A}_{e=1}^{N_{el}}$ is the assembly operator, and the index e is the element number. The entries of the element matrices $m^e = [m_{ij}^e]$, $c^e = [c_{ij}^e]$, and $k^e = [k_{ij}^e]$, and of the element vectors $\boldsymbol{q}^e = \{q_i^e\}$ and $\boldsymbol{f}^e = \{f_i^e\}$, are easily obtained from Eq. (9):

$$m_{ij}^e = -\int_{\Omega^e} \frac{1}{r} \phi_i k_\theta \phi_j \, d\Omega \tag{13}$$

$$c_{ij}^e = -\int_{\Omega^e} \frac{1}{r} \phi_i \kappa_\theta \phi_j \, d\Omega \tag{14}$$

$$k_{ij}^e = \int_{\Omega^e} \bar{\nabla} \phi_i \cdot \bar{\kappa} \bar{\nabla} \phi_j r \, d\Omega + \int_{\gamma_H^e} \phi_i \lambda \phi_j r \, d\gamma^e \tag{15}$$

$$q_i^e = \int_{\gamma_H^e} \phi_i C_R \left[\sum_j \phi_j d_j^e(\theta) \right]^4 r \, d\gamma^e \tag{16}$$

$$f_i^e = \int_{\gamma_H^e} \phi_i f r \, d\gamma^e - \tilde{f}_i^e \tag{17}$$

Here, $\phi_i = \phi_i^e$ is the local shape function associated with element node i, γ_H^e is the part of γ_H belonging to element e, and $\boldsymbol{d}^e = \{d_j^e(\theta)\}$ in Eq. (16) is the element solution vector, which is the local counterpart of the global vector $\boldsymbol{d}(\theta)$. The vector $\tilde{\boldsymbol{f}}^e = \{\tilde{f}_i^e\}$ in Eq. (17) is related to the temperature boundary conditions [Eq. (4)], and is defined by

$$\tilde{\boldsymbol{f}}^e = k^e \boldsymbol{g}^e + c^e \dot{\boldsymbol{g}}^e + m^e \ddot{\boldsymbol{g}}^e \tag{18}$$

where $\boldsymbol{g}^e$ is the vector whose entry $g_j^e(\theta)$ is the value of the prescribed temperature g at node j of element e, if this node is on γ_T, and zero otherwise.

Remarkably, the FE nonlinear system of Eq. (11) has a similar form to that obtained in transient analysis,[21] although in the latter context, a superposed dot denotes differentiation with respect to time rather than with respect to the angle θ. The matrices M, C, and K are analogous to the mass, damping, and stiffness matrices, respectively, in transient analysis. All three are symmetric sparse matrices. The matrix K is positive definite, whereas M is negative definite according to Eq. (13). The element-level expressions [Eqs. (13–15)] are clearly nonstandard. System (11) is nonlinear because of the temperature-dependent radiation vector $\boldsymbol{Q}(\boldsymbol{d})$. In addition, as mentioned previously, the thermal conductivities $\bar{\kappa}$ and κ_θ may depend on the temperature, in which case material nonlinearity is present as well.

In the general case, the matrices M, C, and K depend on the angle θ through $\kappa(\theta)$. Thus, the entries of these matrices are periodic functions of θ. However, there are some important special cases. If $\bar{\kappa}$ and κ_θ depend on location but not on temperature, then M, C, and K are explicit periodic functions of θ. If $\bar{\kappa}$ is not a function of θ (although possibly a function of r and z), then M and K are constant matrices. If κ_θ is not a function of θ, then $C = 0$. Of course, if the material is homogeneous, then M and K are constant matrices and $C = 0$.

The solution of the system of ordinary differential equations [Eq. (11)] must be considered next. The method of solution of this system is based on the spectral method devised by Rand and Givoli.[20] In this method, each θ-dependent function in Eq. (11) is decomposed, using the discrete Fourier transform, into a finite number of harmonics, N, and the Fourier coefficients are found using a nonlinear harmonic balance analysis. All of the calculations involved are done symbolically by the computer code itself. See Refs. 4 and 5 for application of this methodology in another context. Finally, one obtains a coupled nonlinear system of algebraic equations for the unknown Fourier coefficients. This system is solved by means of a modified Newton–Raphson iterative procedure.[4]

III. FE Formulation for General Geometries

At this point, the assumption that D is a body of revolution, namely, the assumption of axisymmetric geometry, is relaxed considerably, and the method is extended to more general geometries. Let $r = r_{in}$ and $r = r_{out}$ describe the inner and outer boundaries of D, respectively (see Fig. 1a). In the axisymmetric case r_{in} and r_{out} are functions of z only (see Fig. 1b). In the more general case, which is considered now, r_{in} and r_{out} are allowed to vary with θ as well. The functions $r_{in}(\theta, z)$ and $r_{out}(\theta, z)$ are assumed to be single-valued continuous functions of θ. Then, the geometry of the cross-section Ω in the (r, z) plane (Fig. 1b) depends on θ, and it is appropriate to write $\Omega = \Omega(\theta)$ and $\gamma = \gamma(\theta)$.

Because the domain Ω varies with θ, different FE meshes must be defined for different cross sections. Thus, the nodal coordinates depend on θ, while the mesh topology most conveniently remains fixed. Assuming that the expressions for the boundaries r_{in} and r_{out} are given explicitly as functions of θ, the element nodal coordinates and, hence, the element domains Ω^e and their boundaries γ^e, can also be parameterized explicitly with respect to θ.

A careful examination of the mathematical derivation reveals that in this more general case, all of the expressions given in the previous FE formulation, and in particular in Eqs. (11) and (13–17), remain valid, with the following differences. First, all of the element matrices and vectors depend on θ through the domains of integration in Eqs. (13–17). For each value of θ, these domains of integration are fixed, and the element matrices and vectors can be evaluated. As a result, the global matrices M, C, and K, and vectors $\boldsymbol{Q}$ and $\boldsymbol{F}$, depend on θ because of the varying geometry (possibly, in addition to the dependence on θ because of nonconstant thermal conductivities).

Second, certain modifications are needed in the element-level expressions [Eqs. (14–17)], if the shape of the boundary γ_H depends on θ. The reason is that in this case the normal $\boldsymbol{n}$ to the boundary Γ, which appears in Eq. (3), does not coincide with the normal $\boldsymbol{n}_\gamma$ to the boundary γ, which is implicitly used in deriving the weak Eq. (9) and, thus, the FE equations. Suppose the geometrical relation between $\boldsymbol{n}$ and $\boldsymbol{n}_\gamma$ is given by

$$\boldsymbol{n} = T_1(\theta)\boldsymbol{n}_\gamma + T_2(\theta)\boldsymbol{e}_\theta \tag{19}$$

where $T_1(\theta)$ and $T_2(\theta)$ are given functions, and $\boldsymbol{e}_\theta$ is the unit normal in the angular ($\theta-$) direction. In the axisymmetric case, $T_1 = 1$ and $T_2 = 0$. From Eq. (19), the operator in Eq. (3) can be written as

$$\boldsymbol{n}\cdot\kappa\nabla u = T_1(\theta)\boldsymbol{n}_\gamma\cdot\bar{\kappa}\bar{\nabla}u + \frac{T_2(\theta)}{r}\kappa_\theta\frac{\partial u}{\partial\theta} \tag{20}$$

Using Eq. (20) in the derivation of Eq. (9), it is possible to show that Eqs. (13–17) are replaced by the following expressions:

$$m_{ij}^e = -\int_{\Omega^e}\frac{1}{r}\phi_i\kappa_\theta\phi_j\,\mathrm{d}\Omega \tag{21}$$

$$c_{ij}^e = -\int_{\Omega^e}\frac{1}{r}\phi_i\dot{\kappa}_\theta\phi_j\,\mathrm{d}\Omega + T_1^{-1}(\theta)T_2(\theta)\int_{\gamma_H^e}\phi_i\kappa_\theta\phi_j\,\mathrm{d}\gamma^e \tag{22}$$

$$k_{ij}^e = \int_{\Omega^e}\bar{\nabla}\phi_i\cdot\bar{\kappa}\bar{\nabla}\phi_j r\,\mathrm{d}\Omega + T_1^{-1}(\theta)\int_{\gamma_H^e}\phi_i\lambda\phi_j r\,\mathrm{d}\gamma^e \tag{23}$$

$$q_i^e = T_1^{-1}(\theta)\int_{\gamma_H^e}\phi_i C_R\left[\sum_j\phi_j d_j^e(\theta)\right]^4 r\,\mathrm{d}\gamma^e \tag{24}$$

$$f_i^e = T_1^{-1}(\theta)\int_{\gamma_H^e}\phi_i f r\,\mathrm{d}\gamma^e - \tilde{f}_i^e(\theta) \tag{25}$$

These expressions reduce to Eqs. (13–17) in the axisymmetric case. It is apparent that the extension of the method to asymmetric geometries has the effect of introducing geometrical factors (not unlike the view factors related to the incoming heat flux[20]) in the element matrix k^e and vectors $\boldsymbol{q}^e$ and $\boldsymbol{f}^e$, as well as introducing an additional term in c^e.

Thus, the methodology proposed here is valid for domains that deviate from bodies of revolution. This deviation cannot be carried to an extreme; e.g., local holes or inclusions in the three-dimensional domain D are not allowed. The dependence of the geometry on θ must be continuous and single-valued. Also, so that the method is numerically efficient, D should be sufficiently similar to a body of revolution. In Sec. V, specific examples are given that demonstrate the extent of geometrical flexibility.

IV. FE Formulation: The Two-Dimensional Case

The FE formulation presented in the previous section is now specialized to the two-dimensional case. Namely, the geometry, material properties, and boundary conditions are assumed not to depend on the axial coordinate z. Thus, D is a two-dimensional domain in the (r, θ) plane, and its boundary Γ consists of the two curves $r = r_{\text{in}}(\theta)$ and $r = r_{\text{out}}(\theta)$. The decomposition [Eq. (5)] is used, where for each value of θ, Ω is the interval $r_{\text{in}} \le r \le r_{\text{out}}$, and its boundary γ consists of the two points $r = r_{\text{in}}$ and $r = r_{\text{out}}$. To fix ideas, it is assumed that a prescribed temperature condition [cf. Eq. (4)] is given on $r = r_{\text{in}}$, and a heat-flux condition [cf. Eq. (3)] is given on $r = r_{\text{out}}$, with $\lambda = 0$ (Fig. 2). Thus, in this case $N_{\text{el}} = M = N_{\text{np}} - 1$. Also, for simplicity, the material is assumed to be isotropic and homogeneous, namely, $\kappa_{ij} = \kappa\delta_{ij}$, where κ is a constant thermal conductivity, and δ_{ij} is the Kronecker delta.

In the two-dimensional case, it is easy to obtain explicit expressions for the geometrical factors $T_1(\theta)$ and $T_2(\theta)$ in Eq. (19). Let $r = \rho(\theta)$ be one of the boundaries $r = r_{\text{in}}$ or $r = r_{\text{out}}$, $\boldsymbol{n}$ be the unit normal vector, $\boldsymbol{t}$ be the unit tangent vector, and $\boldsymbol{e}_r$ and $\boldsymbol{e}_\theta$ be the unit vectors in the r and θ directions, respectively. (Fig. 3). Denoting the position vector on $r = \rho(\theta)$ by $\boldsymbol{\rho}(\theta)$, one has

$$\boldsymbol{\rho}(\theta) = \rho(\theta)\boldsymbol{e}_r(\theta) \tag{26}$$

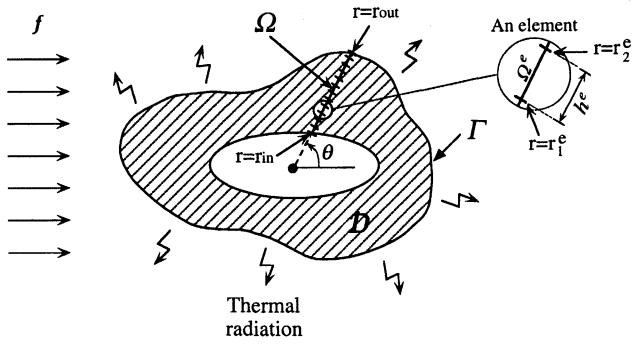

Fig. 2 Setup for the two-dimensional case.

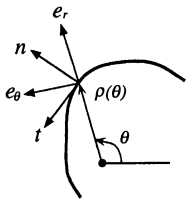

Fig. 3 Boundary $r = \rho(\theta)$ and associated unit vectors.

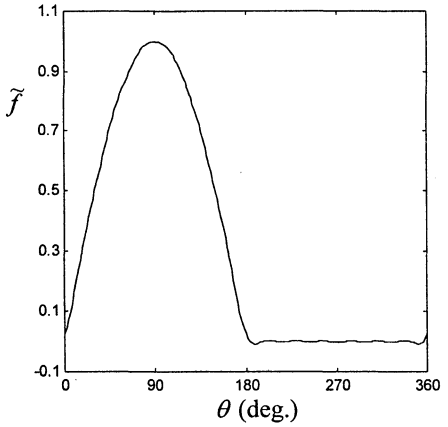

Fig. 4 Prescribed heat flux $\tilde{f}(\theta)$ on the outer boundary, as a result of a unidirectional incoming flux. This half sine-wave is constructed here from its Fourier components by using the first five harmonics.

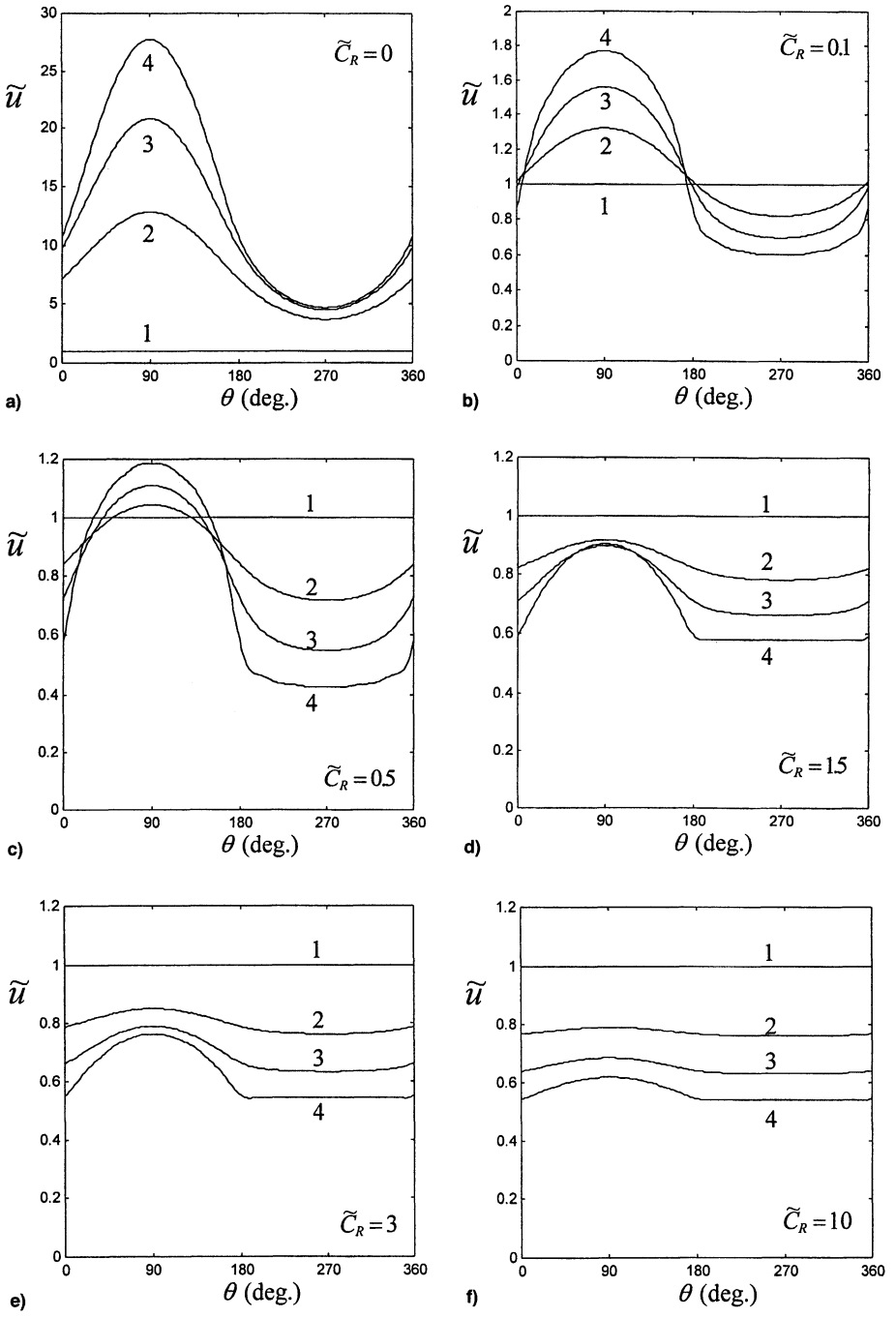

Fig. 5 Axisymmetric geometry with a unidirectional incoming heat flux. Circumferential temperature distribution at four radial locations: $\tilde{r} = r_{in} = 1$ (location 1), $\tilde{r} = 1.1667$ (location 2), $\tilde{r} = 1.4167$ (location 3), and $\tilde{r} = r_{out} = 1.6667$ (location 4). $\tilde{C}_R$ = a) 0, b) 0.1, c) 0.5, d) 1.5, e) 3.0, and f) 10.0.

From differential geometry, the vector $\dot{\boldsymbol{\rho}}(\theta)$ is tangent to the boundary, and $\dot{\boldsymbol{e}}_r(\theta) = \boldsymbol{e}_\theta$. This yields

$$t = \frac{\dot{\boldsymbol{\rho}}}{|\dot{\boldsymbol{\rho}}|} = \frac{\dot{\rho}\boldsymbol{e}_r + \rho\boldsymbol{e}_\theta}{\sqrt{\dot{\rho}^2 + \rho^2}} \tag{27}$$

The normal $\boldsymbol{n}$ can be found from t by using the first Serret–Frenet equation for a curve. However, it is easy to see that $n_r = t_\theta$ and $n_\theta = -t_r$. Therefore

$$\boldsymbol{n} = T_1(\theta)\boldsymbol{e}_r + T_2(\theta)\boldsymbol{e}_\theta \tag{28}$$

where

$$T_1(\theta) = \frac{\rho}{\sqrt{\dot{\rho}^2 + \rho^2}}, \qquad T_2(\theta) = -\frac{\dot{\rho}}{\sqrt{\dot{\rho}^2 + \rho^2}} \tag{29}$$

In this case, the expressions for the element matrices m^e and k^e are

$$m^e_{ij} = -\kappa \int_{\Omega^e} \frac{1}{r}\phi_i\phi_j \, dr \tag{30}$$

$$k^e_{ij} = \kappa \int_{\Omega^e} \phi_i'\phi_j' r \, dr \tag{31}$$

where a prime denotes differentiation with respect to r. The matrix C and the element vectors $\boldsymbol{Q}$ and $\boldsymbol{F}$ are most conveniently obtained directly on the global level:

$$C_{IJ} = T_1^{-1}(\theta)T_2(\theta)\kappa\delta_{IM}\delta_{JM} \tag{32}$$

$$Q_I = T_1^{-1}(\theta)\delta_{IM}C_R r_{out}[d_M(\theta)]^4 \tag{33}$$

$$F_I = T_1^{-1}(\theta)\delta_{IM} r_{\text{out}} f(\theta) - \tilde{F}_I(\theta) \tag{34}$$

Here, M is the degree-of-freedom number corresponding to the node at $r = r_{\text{out}}$, and $\tilde{\boldsymbol{F}} = \{\tilde{F}_I\}$ is the global counterpart of the element vector $\tilde{\boldsymbol{f}}$ defined by Eq. (18), and is calculated by

$$\tilde{F}_I = \delta_{I1}(k^1_{12} g + m^1_{12} \ddot{g}) \tag{35}$$

Consider now the case where the interval $r_{\text{in}} \le r \le r_{\text{out}}$ is divided into $N_{\text{el}} = M$ equal elements, each with two nodes and linear shape functions ϕ_i. Then the integrals in Eqs. (30) and (31) can be evaluated explicitly, and the following expressions are obtained:

$$m^e_{ij} = -\kappa[a^e_{ij}\, \ell n(r^e_2/r^e_1) + b^e_{ij} h^e + p^e_{ij}] \tag{36}$$

$$k^e_{ij} = \kappa p^e_{ij} \tag{37}$$

where

$$\begin{aligned} a^e_{ij} &= (1 - \xi_i r^e_i/h^e)(1 - \xi_j r^e_j/h^e) \\ b^e_{ij} &= (1 - \xi_i r^e_i/h^e)\xi_j/h^e + (1 - \xi_j r^e_j/h^e)\xi_i/h^e \\ p^e_{ij} &= [(r^e_2)^2 - (r^e_1)^2]\xi_i\xi_j/[2(h^e)^2], \qquad \xi_1 = -1,\ \xi_2 = 1 \\ h^e &= r^e_2 - r^e_1 = (r_{\text{out}} - r_{\text{in}})/N_{\text{el}} \end{aligned} \tag{38}$$

If $r = r_{\text{in}}$ and $r = r_{\text{out}}$ are circles, then the matrices M and K are constant, and C vanishes, whereas $\boldsymbol{Q}$ and $\boldsymbol{F}$ depend on θ because of the asymmetries in the thermal loading. If $r = r_{\text{in}}(\theta)$ or $r = r_{\text{out}}(\theta)$ are noncircular, then all of the element quantities in Eq. (38) are functions of θ because of the geometrical asymmetry. As a result, M, C, and K depend on θ as well.

V. Numerical Examples

The FFE method described in Secs. II–IV is applied to a number of examples in two dimensions (see Fig. 2). As in Sec. IV, it is assumed that the temperature is prescribed on $r = r_{\text{in}}$, and a heat-flux condition is given on $r = r_{\text{out}}$, with $\lambda = 0$, and that the material is isotropic and homogeneous. The interval $\Omega = (r_{\text{in}}, r_{\text{out}})$ is divided into equally sized two-node linear elements, and Eqs. (32–38) are used.

To present the results in a unit-independent way, all of the equations are nondimensionalized. The nondimensional quantities are defined as follows:

$$\begin{aligned} &\tilde{r} = r/r_0, \quad \tilde{r}_{\text{in}} = r_{\text{in}}/r_0, \quad \tilde{r}_{\text{out}} = r_{\text{out}}/r_0, \quad \tilde{u} = u/u_0 \\ &\tilde{f} = f/f_0, \quad \tilde{g} = g/u_0, \quad \tilde{\kappa} = u_0\kappa/(r_0 f_0), \quad \tilde{C}_R = u_0^4 C_R/f_0 \end{aligned} \tag{39}$$

where r_0 is a reference length, u_0 is a reference temperature, and f_0 is a reference heat flux. In the present case, r_0 is chosen to be the average of $r_{\text{in}}(\theta)$, u_0 is the maximal value of g, and f_0 is the maximal value of f.

First, an axisymmetric problem is considered for which an analytic solution can be obtained. The domain D is a ring (or the wall of an infinite cylinder) bounded by $\tilde{r}_{\text{in}} = 1$ and $\tilde{r}_{\text{out}} = 5$. The prescribed temperature on the inner boundary is $\tilde{g} \equiv 1$, and the incident heat flux on the outer boundary is $\tilde{f} \equiv 1$.

In the linear case, when $\tilde{C}_R = 0$, the exact solution is given by

$$\tilde{u}(\tilde{r}) = \tilde{g} + (\tilde{r}_{\text{out}}\tilde{f}/\tilde{\kappa})\ell n(\tilde{r}/\tilde{r}_{\text{in}}) = 1 + (5/\tilde{\kappa})\ell n\, \tilde{r} \tag{40}$$

The FFE method, with $\tilde{\kappa} = 0.2$ and $N_{\text{el}} = 8$, in this case yields a relative error of about 0.5%. In the nonlinear case, when $\tilde{C}_R \neq 0$, an implicit analytic solution can still be obtained by the following procedure. Let $q(\tilde{u}) \equiv 1 - \tilde{C}_R\tilde{u}^4$ be the total normal heat flux on the outer boundary. Then the temperature on the outer boundary, $u_{\text{out}} \equiv \tilde{u}(\tilde{r}_{\text{out}})$ can be deduced from Eq. (40):

$$u_{\text{out}} = \tilde{g} + \frac{\tilde{r}_{\text{out}} q(u_{\text{out}})}{\tilde{\kappa}}\, \ell n\left(\frac{\tilde{r}}{\tilde{r}_{\text{in}}}\right) = 1 + \frac{5q(u_{\text{out}})}{\tilde{\kappa}}\, \ell n\, 5 \tag{41}$$

On the other hand, from the definition of q

$$\tilde{C}_R = [1 - q(u_{\text{out}})]/u^4_{\text{out}} \tag{42}$$

Equations (41) and (42) can be used to obtain the graph of u_{out} as a function of $\tilde{C}_R$. A single point in this graph is obtained by choosing a value of $q(u_{\text{out}})$, substituting in Eq. (41) and finding u_{out}, and then substituting in Eq. (42) and obtaining the corresponding value of $\tilde{C}_R$. A similar graph has been obtained numerically by the FFE method. This has been done for various values of $\tilde{\kappa}$. The relative difference between the analytic and numerical solution was again found to be about 0.5%.

Next, an asymmetric thermal loading is considered, with the axisymmetric geometry of the previous example. The normal heat flux prescribed on $\tilde{r} = \tilde{r}_{\text{out}}$ is that generated by a unidirectional incoming flux, such as solar radiation, directed in the $\theta = -90$-deg direction. Because of the circular geometry of the boundary and the self-shading of the cylinder, a half sine-wave view factor multiplies the nominal constant incoming flux,[20] i.e., $\tilde{f}(\theta) = \max\{\sin\theta, 0\}$. In the numerical scheme, a fast

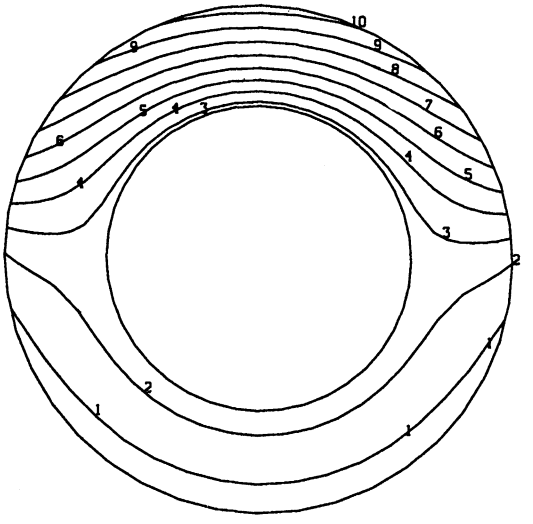

Fig. 6 Axisymmetric geometry with a unidirectional incoming heat flux; $\tilde{C}_R = 0.1$: isotherms ["1" = 0.86, "10" = 1.66].

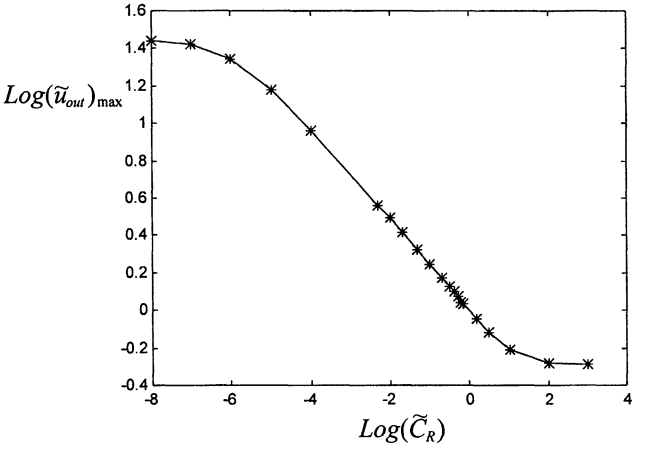

Fig. 7 Axisymmetric geometry with a unidirectional incoming heat flux: maximal temperature on the outer boundary as a function of $\tilde{C}_R$.

Fourier transform scheme is used to decompose $\tilde{f}$ into its Fourier modes. $N = 12$ modes were used in the present case throughout the analysis. Figure 4 shows the function $\tilde{f}(\theta)$ as reconstructed from its first 12 modes. It is clear that the Fourier representation of the loading function is quite satisfactory, despite the fact that $\tilde{f}(\theta)$ is not smooth, i.e., not differentiable at $\theta = 0$ and $\theta = \pi$. The other fixed parameters in this example are $\tilde{r}_{in} = 1$, $\tilde{r}_{out} = 1.6667$, $\tilde{g} \equiv 1$, $\tilde{\kappa} = 0.2$, and $N_{el} = 8$.

Figures 5a–5f show the temperature $\tilde{u}$ as a function of θ in four radial locations: $\tilde{r} = r_{in} = 1$ (location 1), $\tilde{r} = 1.1667$ (location 2), $\tilde{r} = 1.4167$ (location 3), and $\tilde{r} = r_{out} = 1.6667$ (location 4). Each figure corresponds to a different value of the radiation constant $\tilde{C}_R$. It is apparent that as the radiation effect is increased, the circumferential temperature distribution becomes more uniform. Thus, when no thermal radiation is present (Fig. 5a), the results depend strongly on θ, whereas when $\tilde{C}_R$ is large (Fig. 5f), the results very weakly depend on the angular location. The reason is that when the radiation effect is strong, most of the θ-dependent incident heat flux is radiated back out, only slightly affecting the internal temperature distribution in the cylinder.

In addition, the amount of radiation affects the nature of the radial temperature distribution: without radiation (Fig. 5a) the temperature increases everywhere monotonically with r; with small radiation (Figs. 5b–5d) the outer temperature is either larger or smaller than the inner temperature, depending on the angular location; whereas with large radiation (Figs. 5e and 5f), the temperature monotonically decreases everywhere with r. This behavior is also related to the cancellation of part of the incident flux by the radiation effect.

Figure 6 shows the isotherms in the cylindrical wall for $\tilde{C}_R = 0.1$. Here, and in all of the following isotherm plots, 10 level lines are shown that are labeled 1–10, and which represent equally spaced temperature values between the minimum and maximum values. In the present case, the maximal temperature is 1.7, and is achieved at the top of the outer boundary (where the incoming heat flux is maximal). The maximal temperature on the outer boundary as a function of $\tilde{C}_R$ is shown in Fig. 7 in a logarithmic scale. The highest value, which is $\tilde{u} = 27.7$, is obtained when no thermal radiation is present, as expected. The lowest value is $\tilde{u} = 0.54$, which is approached asymptotically when $\tilde{C}_R \to \infty$.

Now an asymmetric geometry is considered. While the outer boundary remains the circle $\tilde{r}_{out} = 1.6667$, the inner boundary is defined by the function $\tilde{r}_{in}(\theta) = 1 + 0.333 \cos \theta$, which approximately represents a circle shifted by 0.333 to the right. The other fixed parameters are $\tilde{g} \equiv 1$, $\tilde{\kappa} = 0.2$, $N_{el} = 8$, and $N = 10$. First, the case $\tilde{f} \equiv 1$, $\tilde{C}_R = 0$ is considered. Here, the only asymmetry in the problem is that because of the geometry. For this case, a standard two-dimensional FE model has been used to obtain results of the same problem to compare them with those obtained by the proposed FFE method. Figure 8a illustrates the FE mesh used in the standard model, which consists of 320 elements and 360 nodes.

Figures 8b and 8c are, respectively, the isotherm plots obtained by the standard FE method and the FFE method. It is clear that the agreement between the two results is excellent. Quantitative comparison shows that the pointwise differences between the two solutions are smaller than 3.5%. It should be remarked that the largest error occurs in the leftmost part of the domain, where a slight discrepancy in the isotherms can be seen by comparing Figs. 8b and 8c. This can be explained by the fact that the solution in the region that is relatively close to the inner boundary is more strongly affected by the prescribed temperature on this boundary. This leads to a larger error in the region that is relatively remote from the inner boundary.

The last experiment confirms the correctness of the FFE scheme. It also serves to compare the efficiency of the FFE

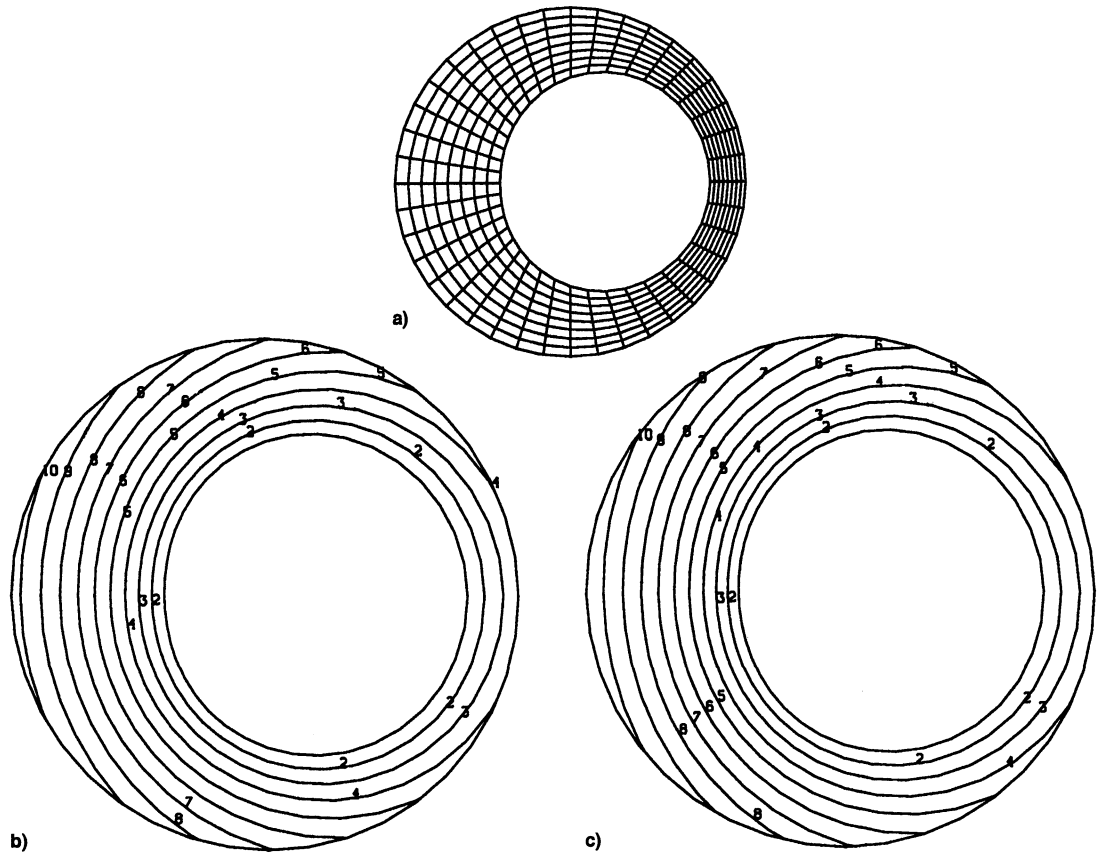

Fig. 8 Asymmetric geometry (shifted inner boundary), no radiation, uniform incident heat flux: a) FE mesh in the standard FE scheme; b) isotherms obtained by the FE scheme ["1" = 1.0, "10" = 7.30]; and c) isotherms obtained by the FFE scheme ["1" = 1.0, "10" = 7.30].

and standard FE schemes. The FFE scheme, with $M \times (2N + 1) = 168$ degrees of freedom, achieves the same accuracy as the FE scheme that uses 320 degrees of freedom. Of course, this is not always the case; in problems where the solution is not sufficiently smooth in the angular direction, the standard FE method may be more efficient. See further discussion of the computational aspects at the end of this section.

Now, the case of a unidirectional incoming flux (cf. Fig. 4) is considered, with the same geometry and with various values of $\tilde{C}_R$. The other parameters remain as before. There are two sources of asymmetry in this case: the geometry and the thermal loading. Figures 9a–9c describe the isotherms obtained for three values of $\tilde{C}_R$. The isotherm patterns are quite different in the three cases. When $\tilde{C}_R$ is small (Fig. 9a), the maximal temperature ($\tilde{u} = 1.7$) is obtained at the top part of the outer boundary, the smallest temperature ($\tilde{u} = 0.79$) occurs at a point on the bottom, whereas the inner boundary is kept at the intermediate temperature $\tilde{u} = 1$. When $\tilde{C}_R$ is increased (Fig. 9b), the maximal temperature is $\tilde{u} = 1$ on the inner boundary, but this isotherm also intersects the outer boundary at two points on the upper part. When $\tilde{C}_R$ becomes very large (Fig. 9c), closed isotherms are obtained, and the maximal temperature $\tilde{u} = 1$ occurs only at the inner boundary.

It is interesting to compare Fig. 6 with Fig. 9a. The only difference between the two problems is that in the former, the two boundaries are concentric, whereas in the latter, they are eccentric. It is clear that aside from the asymmetry inherent in Fig. 9a, the solution is similar qualitatively. This similarity is observed for other values of $\tilde{C}_R$ as well.

Finally, the case of a square hole in a circular domain is considered. The side of the square is of length 1, and the outer radius is $\tilde{r}_{\text{out}} = 1$. Note that the square boundary is represented by a Fourier expansion, as are all of the other θ-dependent quantities in the problem. The other fixed parameters are, $\tilde{f}$ is defined by the half sine-wave (Fig. 4), $\tilde{g} \equiv 1$, $\tilde{\kappa} = 0.2$, $N_{\text{el}} = 8$, and $N = 10$. Figures 10a–10c depict the isotherms for three values of $\tilde{C}_R$. The behavior of the solution is similar in nature to that observed in the previous example.

It should be noted that the domain D in the last example contains four re-entrant corners, which are singularity points. The normal derivative of the exact solution is not bounded in these points. In the present analysis, these singularities were simply ignored. However, a more accurate analysis requires special treatment of these singularities. Perhaps the simplest way to account for them is by refining the mesh locally near the four corners. This can be done very easily in the FFE method: it only requires the adaptation of a one-dimensional FE mesh, and an appropriate increase in the number of harmonics.

We close this section with a brief discussion of some computational aspects of the FFE method. A detailed description of the relative advantages and disadvantages of the method compared to standard FE analysis may be found in Ref. 4, where the Fourier decomposition is applied in time, and in Ref. 20, where it is applied in space.

As indicated in Sec. I, an important advantage of FFE is the dimensional reduction of the FE model. One consequence of this reduction is that the meshing process must be done in a smaller dimension. In addition, refining or adapting the mesh in the case of an adaptive scheme becomes easier in the FFE method. For example, in the two-dimensional case considered in this section, constructing and refining the FFE mesh is a trivial task, whereas the FE user has to maintain good aspect ratios for all of the elements while generating or adapting the mesh. In the FFE method, controlling the accuracy in the tangential direction is done independently of the other spatial directions; simply a larger number of harmonics, N, must be taken, and there is no need in remeshing or reforming the element arrays. These advantages become even more distinct in three dimensions.

The accuracy of the FFE method, compared with that of the standard FE method, depends mainly on the smoothness of the exact solution in the angular direction. If the solution is infinitely smooth in this direction, then the FFE method yields results that are much more accurate. This is generally the case with global spectral schemes or with spectral or p-type FE schemes that lead to an exponential rate of convergence, as opposed to standard h-type FE schemes that are associated with algebraic convergence.[10] On the other hand, if the exact solution has a low degree of regularity, e.g., suffers from dis-

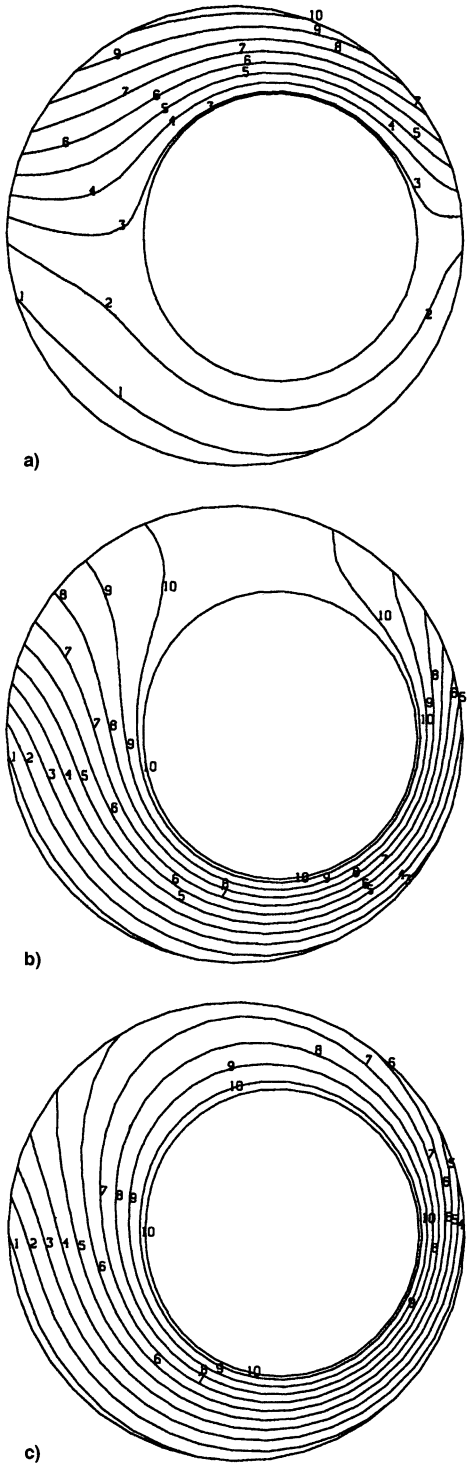

Fig. 9 Asymmetric geometry (shifted inner boundary), unidirectional incoming heat flux: isotherms. $\tilde{C}_R$ = a) 0.1 ["1" = 0.84, "10" = 1.66]; b) 1 ["1" = 0.55, "10" = 0.98]; and c) 3 ["1" = 0.45, "10" = 0.97].

continuities or jumps in slope in the angular direction, then the standard FE method would yield more accurate results for the same number of degrees of freedom. Thus, the choice of one method over the other is problem dependent.

There are three main sources of errors in the FFE method: 1) the FE discretization error, 2) the error generated by truncating the Fourier expansion after N terms, and 3) the geometrical error that is generated if the domain under consideration deviates from that of a body of revolution. The latter error is related to the fact that while taking the derivative with respect to θ in Eqs. (21–25), r is assumed to be constant, whereas, in fact, r is not constant on a circumferential line if the geometry is noncircular. This means that one has to be careful when applying the method to domains that substantially deviate from a body of revolution.

The calculations that yield the coefficient matrix in the FFE method are performed very efficiently using the symbolic procedures described in Refs. 4 and 5. As a result, the intensive part of the computation is associated with the solution of the final system of nonlinear algebraic equations. For the same number of degrees of freedom, the CPU time and storage requirement in the FFE and standard FE methods are comparable.

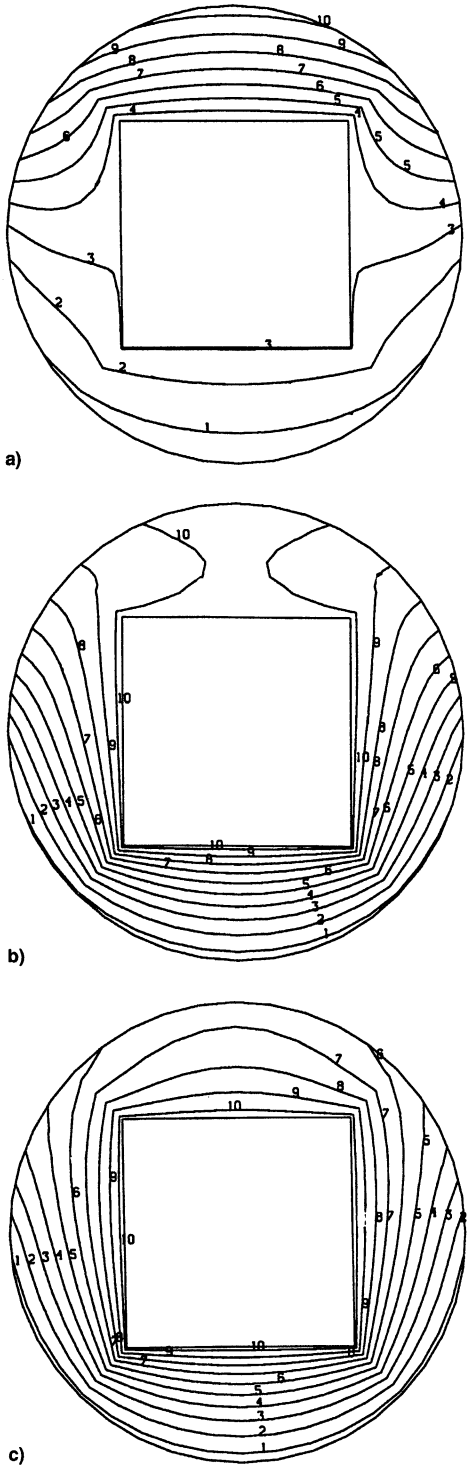

Fig. 10 Square inner boundary, unidirectional incoming heat flux: isotherms. $\tilde{C}_R$ = a) 0.1 ["1" = 0.80, "10" = 1.69]; b) 1 ["1" = 0.51, "10" = 0.97]; and c) 3 ["1" = 0.42, "10" = 0.97].

VI. Concluding Remarks

In this paper, a new numerical method was devised for the solution of nonlinear steady-state heat transfer problems in bodies whose boundaries can be described uniquely in cylindrical coordinates. The method combines symbolically implemented Fourier decomposition in the angular direction and FE discretization in the other spatial directions. In contrast to previously proposed schemes, the present method allows the geometry itself, as well as the material properties and boundary conditions (loading), to be functions of the angular coordinate. Thus, the method constitutes a generalization of standard FE Fourier analysis to nonlinear problems with asymmetric geometry and material properties. Applications include thermal analysis of space structures, or structural members in space structures when detailed local analysis is required.

The method has been demonstrated by solving several two-dimensional problems. In two dimensions, comparison to standard FE calculations is easily performed and, thus, the success of the new scheme can be measured readily. However, the advantages of the method become more distinct in the three-dimensional case, which is currently being implemented. In this case, the scheme requires only the construction of a two-dimensional FE mesh, as opposed to the three-dimensional mesh required in standard FE analysis. An additional future research direction is the adaptation of the method to problems of flexible structures with geometrical and material nonlinearities. In particular, effort will be made in three application areas: 1) more complex heat transfer problems such as three-dimensional time-dependent conduction–radiation problems of large space structures, 2) the thermoelastic analysis of flexible space structures, and 3) the thermoelastic control of twist in helicopter rotor blades. Results of these extensions will be reported in a future publication.

Acknowledgments

This work was partly supported by the Albert Fund for R&D in Aerospace Engineering, by the Adler Fund managed by the Israel Academy of Sciences, and by the Fund for the Promotion of Research at the Technion.

References

[1]Kohl, T., Datta, S. K., and Shah, A. H., "Axially Symmetric Pulse Propagation in Semi-Infinite Hollow Cylinders," *AIAA Journal*, Vol. 30, No. 6, 1992, pp. 1617–1624.

[2]Rand, O., "Periodic Response of Thin-Walled Composite Helicopter Rotor Blades," *Journal of the American Helicopter Society*, Vol. 36, No. 4, 1991, pp. 3–11.

[3]Kalinowski, A. J., and Wachman, M., "Combined Finite Element Method and Spectral Method for Shear Flow-Structure Interaction Problems," *Proceedings of the ASME Winter Annual Meeting* (New Orleans, LA), Vol. 178, American Society of Mechanical Engineers, New York, 1993, pp. 65–79.

[4]Rand, O., and Givoli, D., "A Finite Element Spectral Method with Application to the Thermoelastic Analysis of Space Structures," *International Journal of Numerical Methods in Engineering*, Vol. 30, No. 2, 1990, pp. 291–306.

[5]Givoli, D., and Rand, O., "Thermoelastic Analysis of Space Structures in Periodic Motion," *Journal of Spacecraft and Rockets*, Vol. 28, No. 4, 1991, pp. 457–464.

[6]Givoli, D., and Rand, O., "Minimization of the Thermoelastic Deformation in Space Structures Undergoing Periodic Motion," *Journal of Spacecraft and Rockets*, Vol. 32, No. 4, 1995, pp. 662–669.
[7]Amon, C. H., "Spectral Element-Fourier Method for Transitional Flows in Complex Geometries," *AIAA Journal*, Vol. 31, No. 1, 1993, pp. 42–48.
[8]Amon, C. H., "Spectral Element-Fourier Method for Unsteady Conjugate Heat Transfer in Complex Geometry Flows," *Journal of Thermophysics and Heat Transfer*, Vol. 9, No. 2, 1995, pp. 247–253.
[9]Babuška, I., and Melenk, J. M., "The Partition of Unity Method," *International Journal of Numerical Methods in Engineering*, Vol. 40, 1997, pp. 727–758.
[10]Szabo B., and Babuška I., *Finite Element Analysis*, Wiley, New York, 1991.
[11]Kim, J. R., Kim, W. D., and Kim, S. J., "Parallel Computing Using Semianalytical Finite Element Method," *AIAA Journal*, Vol. 32, No. 5, 1994, pp. 1066–1071.
[12]Thurston, G. A., and Sistla, R., "Elimination of Gibbs' Phenomena from Error Analysis of Finite Element Results," *AIAA Journal*, Vol. 29, No. 12, 1991, pp. 2233–2239.
[13]Kumar, V., and Singh, A. V., "Approximate Vibrational Analysis of Noncircular Cylinders Having Varying Thickness," *AIAA Journal*, Vol. 30, No. 7, 1992, pp. 1929–1931.
[14]Givoli, D., and Libai, A., "Incremental Stresses in Loaded Orthotropic Circular Membrane Tubes—II. Numerical Solution," *Solids and Structures*, Vol. 32, No. 13, 1995, pp. 1927–1947.
[15]Givoli, D., and Rand, O., "Harmonic Finite Element Thermoelastic Analysis of Space Frames and Trusses," *Journal of Thermal Stresses*, Vol. 16, No. 3, 1993, pp. 233–248.
[16]Kaiser, T. M. V., Elwi, A. E., and Mioduchowski, A., "Nonlinear Harmonic Analysis Applied to Axisymmetric Structures," *Computers and Structures*, Vol. 55, No. 6, 1995, pp. 1107–1118.
[17]Danielson, K. T., and Tielking, J. T., "Fourier Continuum Finite Elements for Large Deformation Problems," *Computers and Structures*, Vol. 49, No. 1, 1993, pp. 133–147.
[18]Marusak, R. E., and Becker, E. B., "Finite Element Procedure for Axisymmetric Elastomeric Solids Under General Loading," *International Journal of Numerical Methods in Engineering*, Vol. 36, No. 12, 1993, pp. 2031–2048.
[19]Peshkam, V., and Delpak, R., "Variational Approach to Geometrically Nonlinear Analysis of Asymmetrically Loaded Rotational Shells—II. Finite Element Application," *Computers and Structures*, Vol. 46, No. 1, 1993, pp. 1–11.
[20]Rand, O., and Givoli, D., "Thermal Analysis of Space Structures Including Three-Dimensional Effects," *International Journal of Numerical Methods for Heat and Fluid Flow*, Vol. 2, No. 2, 1992, pp. 115–125.
[21]Hughes, T. J. R., *The Finite Element Method*, Prentice–Hall, Englewood Cliffs, NJ, 1987.

International Reference Guide to Space Launch Systems, Second Edition

Steven J. Isakowitz, editor
Updated by Jeff Samella

This 2nd edition to the best-selling reference guide contains updated and expanded material on launch programs in China, Europe, India, Israel, Japan, Russia/Ukraine, and the United States.

Packed with illustrations and figures, the second edition of the guide is a quick and easy data retrieval source for policy makers, planners, engineers, and students.

Eight standard sections describe each of the launch systems in detail, including: chronological illustrations of production status; vehicle descriptions and their technical differences; a brief text history of the launch system and the launch record; price data; performance curves for a variety of orbits; launch site; launch facilities, launch processing; and flight sequence; payload accommodations; and more.

1995, 341 pp, illus. Softcover
ISBN 1-56347-129-9
AIAA Members: $39.95
List Price: $70.00

AIAA

American Institute of Aeronautics and Astronautics
Publications Customer Service, 9 Jay Gould Ct., P.O. Box 753, Waldorf, MD 20604
Fax 301/843-0159 Phone 800/682-2422 8 a.m. –5 p.m. Eastern

CA and VA residents add applicable sales tax. For shipping and handling add $4.75 for 1–4 books (call for rates for higher quantities). All individual orders, including U.S., Canadian, and foreign, must be prepaid by personal or company check, traveler's check, international money order, or credit card (VISA, MasterCard, American Express, or Diners Club). All checks must be made payable to AIAA in U.S. dollars, drawn on a U.S. bank. Orders from libraries, corporations, government agencies, and university and college bookstores must be accompanied by an authorized purchase order. All other bookstore orders must be prepaid. Please allow 4 weeks for delivery. Prices are subject to change without notice. Returns in sellable condition will be accepted within 30 days. Sorry, we can not accept returns of case studies, conference proceedings, sale items, or software (unless defective). Non-U.S. residents are responsible for payment of any taxes required by their government.